HEAT TRANSFER IN MICROGRAVITY

The 1993 ASME Winter Annual Meeting
New Orleans, Louisiana
November 28 - December 3, 1993

sponsored by
The Heat Transfer Division, ASME

edited by
C. Thomas Avedisian
Cornell University

V. A. Arpaci
University of Michigan

AMERICAN SOCIETY OF MECHANICAL ENGINEERS
ENGINEERING CENTER / 345 EAST 47TH STREET / NEW YORK, NY

HTD-Vol. 269, Heat Transfer in Microgravity
ASME 1993

DIELECTRIC FLUID SOLIDIFICATION WITH CHARGED PARTICLES IN ELECTRIC FIELDS AND REDUCED GRAVITY

George S. Dulikravich and Vineet Ahuja
Department of Aerospace Engineering
Pennsylvania State University
University Park, Pennsylvania

ABSTRACT

A mathematical model and an explicit finite difference iterative integration algorithm for two-dimensional laminar steady flow of an incompressible viscous electrically conducting but neutrally charged liquid containing electrically charged particles and exposed to an externally applied electrostatic field were developed. The system of governing electrohydrodynamic equations was derived from a combination of Maxwell's equations of electrodynamics and the Navier-Stokes equations. An idealized charged fluid was assumed thus making magnetic fields negligible so that the Maxwell's equations reduce to a charge conservation equation and an equation for the electric potential. Thermally induced buoyancy was incorporated via an extended Boussinesq approximation while including Joule heating due to induced electrical current. Latent heat of phase change during melting/solidification was incorporated using an enthalpy method that accounts for mushy region by varying viscosity and electric charge mobility by orders of magnitude between liquidus and solidus. Numerical results demonstrate the existence of strong electro-thermoconvective motion in the liquid during the solidification/melting and quantify its influence on the amount of accrued solid, deposition pattern of the electrically charged particles inside the accrued solid, and the melt/solid interface shape. There is clearly a stronger influence of the applied electric field in reduced gravity than under terrestrial conditions. This suggests an attractive actively controlled solidification process involving dielectric fluids in reduced gravity. It also offers for a possibility to layer the crystals grown from a melt with electrically charged particles. The control algorithm could also be used for predicting the deposition pattern of electrically charged dopants or impurities inside a crystal grown from the melt.

NOMENCLATURE

b	= charged particle mobility coeff.$[m^2 s^{-1} V^{-1}]$
c	= specific heat coefficient $[m^2 K^{-1} s^{-2}]$
D	= charged particle diffusivity coeff. $[m^2 s^{-1}]$
$\mathbf{D}^*$, $\mathbf{D}^*_{NS}$	= diagonal matrices
$E=E(E_x,E_y)$	= electric field vector $[V m^{-1}]$
$\mathbf{E}$	= x-flux vector in Cartesian coordinates
$\mathbf{F}$	= y-flux vector in Cartesian coordinates
$\mathbf{g}=\mathbf{g}(g_x,g_y)$	= gravity acceleration vector $[m s^{-2}]$
$\mathbf{I}$	= identity matrix
k	= heat conductivity coefficient $[kg m s^{-3} K^{-1}]$
k_B	= Boltzman's constant $[kg^{-1} s K]$
l	= length [m]
L	= latent heat of solidification $[J kg^{-1}]$
p	= fluid pressure $[N m^{-2}]$
$\mathbf{Q}$	= solution vector in Cartesian coordinates
q	= electric charge/volume $[kg m^{-1} s^{-2} V^{-1}]$
$\tilde{\mathbf{R}}$	= residual vector
$\mathbf{S}$	= source term vector
T	= temperature [K]
t	= time [s]
$\mathbf{v}=\mathbf{v}(u,v)$	= velocity vector in Cartesian coord. $[m s^{-1}]$
x,y	= Cartesian coordinates [m]
α	= thermal expansion coefficient $[K^{-1}]$
β	= artificial compressibility coefficient
ε	= electric permitivity coeff.$[kg m s^{-2} V^{-2}]$
ε_4	= fourth-order artificial dissipation coeff.
ϕ	= gravity potential $[m^{-2} s^{-2}]$
φ	= electric potential [V]
μ	= dynamic viscosity coefficient $[kg m^{-1} s^{-1}]$
ψ	= artificial dissipation sensor function

ρ = fluid density [kg m^{-3}]
θ = non-dimensional temperature difference

Superscripts
* = non-dimensional quantity
' = function of non-dimensional temperature
T = transpose of a matrix or a vector

Subscripts
cold = cold wall
hot = hot wall
o = reference values
l = liquid
liquidus = liquidus
s = solid
solidus = solidus
E = electrical
, = differentiation

INTRODUCTION

Fluid flow under the influence of a combined electromagnetic field (Landau and Lifshitz, 1960) can be described by two extreme models: electrohydrodynamics (EHD) or magnetohydrodynamics (MHD). The EHD model assumes a quasi-static electric field applied to a fluid containing electrically charged particles and having negligible magnetic induction effects (Stuetzer, 1962; Melcher, 1981; Babski et al., 1989). The phenomenon of electrohydrodynamic instability or the generation of vorticity resulting from a non-uniform electric charge distribution in the fluid under the influence of an electric field is well known (Landau and Lifshitz, 1960). This is due to the existence of the Coulomb forces (Eringen and Maugin, 1990) that arise from the interaction of the electric charges and the electric potential energy.

A number of experimental observations and several simplified analytical studies have been performed on the general topic of interaction of electroconvection and heat transfer. A comprehensive review of the operational principles of the EHD in single phase and condensation heat exchangers is provided by Ohadi (1991). For example, the injection of charges between two electrodes was dealt with in detail by Zahn and Chatelon (1977). The EHD enhancement of heat transfer has been demonstrated by Fujino et al (1989) for flows between parallel plates. Investigations by Fernandez and Poulter (1987) revealed the enhancement of heat transfer rates exhibited by liquids flowing in ducts when subjected to an electrostatic potential. Several incomplete models of EHD flows without phase change have been numerically solved in the past (Belo and Polezhaev, 1991; Lee, Dulikravich and Kosovic, 1991; Dulikravich, Ahuja and Lee, 1993a; 1993b). The main reason is the extreme complexity of the physical phenomena and the corresponding mathematical models (Babski et al., 1989; Hosseini-Sianaki et al., 1992; Dulikravich and Kosovic, 1992; Dulikravich, Ahuja and Lee, 1993a). On the other hand, several recent publications addressed simulation of MHD solidification under the influence of a reduced gravity (Dulikravich and Kosovic, 1992; Dulikravich, Ahuja and Lee, 1993c).

This paper represents a more thorough and precise analytical model of EHD solidification/melting than in our earlier work (Dulikravich and Kosovic, 1992). Specifically, here we elaborate on a single set of partial differential equations capable of describing the entire phenomena not only in the all melt regions, but also in the mushy (mixed melt and solid) regions, as well as in the all solid regions. This is possible by modeling the solid phase as been yet another liquid having all physical properties of the actual solid, except for its viscosity which will be extremely high but finite. In such a way, the actual solid phase regions will be computationally predicted as regions having practically zero internal velocity field. For the purpose of clarity, we will often refer to the melt as "liquid" and to the extremely viscous fluid as "solid".

A detailed numerical investigation of the impact of the EHD on the distribution of surface heat fluxes during solidification in reduced gravity and in terrestrial conditions will be presented for a simple case of a closed two-dimensional container. The results demonstrate the significant influence that this fundamental phenomena has on heat transfer enhancement, the amount of accrued solid, the deposition pattern of the charged particles inside the solid, and the liquid/solid interface shape.

EHD SOLIDIFICATION: ANALYTICAL MODEL

The mathematical model presented in this paper consists of an electrically neutral, homocompositional, viscous, incompressible liquid that is seeded with one type of charged particles having all physical properties identical to those of its immediate neighbourhood media (all liquid, mushy region, or all solid) except that the particles are electrically charged. This model can be extended to electrically non-neutral liquids and solids and multiple-specie charged particles having different physical properties. In this paper, the objective is to demonstrate only fundamental effects of the applied electrostatic field for which a single-specie formulation will suffice. Although many practical solidification/melting processes involve turbulent flows, we have decided to study solidification/melting with EHD effects in laminar flows only, since reliable and universal turbulence models for EHD flows do not exist. We will also assume that there is no electrolysis or pool boiling in the liquid and that charged particles do not undergo chaining (no electro-rheological effects).

The system of governing equations for EHD can be derived from a combination of Maxwell's equations of electrodynamics and the Navier-Stokes equations (Lee, Dulikravich and Kosovic, 1991; Dulikravich, Ahuja and Lee, 1993a; 1993b). An idealized charged fluid is assumed (Stuetzer, 1962; Melcher, 1981) and, therefore, induced magnetic fields can be neglected. In the same model, the magnetic field vector and the electric polarization vector are assumed negligible compared to the electric field vector. Consequently, Maxwell's equations can be reduced to an electric charge conservation equation and a Poisson's partial differential equation for electric potential since the electric field is irrotational.

Starting with the complete Navier-Stokes equations for compressible fluid flow and assuming that density variations

as a function of temperature are small, an extended form of the Boussinesq approximation can be derived for the fluids with temperature-dependent properties (Gray and Giorgini, 1976; Lee, Dulikravich and Kosovic, 1991). Thus, the EHD governing equations are:
Mass conservation

$$\nabla \cdot \mathbf{v} = 0 \tag{1}$$

Linear momentum conservation (including thermal buoyancy force and electrostatic Coulomb force)

$$\rho \frac{D\mathbf{v}}{Dt} = -\nabla p - \rho\, \alpha\, \mathbf{g}\, \Delta T + \nabla \cdot \left(\mu(\nabla \mathbf{v} + (\nabla \mathbf{v})^T)\right) + q\, \boldsymbol{E} \tag{2}$$

Energy conservation (including Joule heating)

$$\rho\, c\, \frac{DT}{Dt} = \nabla \cdot (k\, \nabla T) + \mathbf{J} \cdot \boldsymbol{E} \tag{3}$$

Electric charge conservation

$$\frac{\partial q}{\partial t} + \nabla \cdot \mathbf{J} = 0 \tag{4}$$

Electric potential field

$$\nabla \cdot \boldsymbol{E} = \frac{q}{\varepsilon} \tag{5}$$

Notice that the induced electric current per unit volume is given by Ohm's law (including a charge diffusion term)

$$\mathbf{J} = q\,(\mathbf{v} + b\,\boldsymbol{E}) - D\,\nabla q \tag{6}$$

The electric charge diffusivity coefficient D and charge mobility coefficient b are related by Einstein's formula (Melcher, 1981)

$$D = \frac{k_B\, T\, \rho_i}{q\, m_i}\, b \tag{7}$$

where m_i is the mass of a charged particle and ρ_i is the density of the electrically charged particles. Since the electric field is irrotational, it follows that

$$\boldsymbol{E} = -\nabla \varphi \tag{8}$$

Here, φ is the electric potential so that equation (8) becomes

$$\nabla^2 \varphi = -\frac{q}{\varepsilon} \tag{9}$$

Non-dimensionalization can be performed with respect to the reference values denoted by subscript "o", so that

$$\mathbf{v}^* = \frac{\mathbf{v}}{|\mathbf{v}_o|} \quad \mathbf{x}^* = \frac{\mathbf{x}}{l_o} \quad t^* = \frac{t|\mathbf{v}_o|}{l_o} \quad p^* = \frac{p}{\rho_o |\mathbf{v}_o|^2} \tag{10}$$

$$\varphi^* = \frac{\Delta\varphi}{\Delta\varphi_o} \quad \boldsymbol{E}^* = \frac{\boldsymbol{E}\, l_o}{\Delta\varphi_o} \quad q^* = \frac{q}{q_o} \quad \theta = \frac{T - T_o}{\Delta T_o} \quad \mathbf{g}^* = \frac{\mathbf{g}}{|\mathbf{g}_o|} \tag{11}$$

Typically, if T_{cold} is the temperature of the cold wall and T_{hot} is the temperature of the hot wall, then $\Delta T_o = T_{hot} - T_{cold}$ where T_o is often taken as the solidus temperature, that is $T_o = T_{solidus}$. Similarly, $\Delta\varphi_o$ is the reference value of the electric potential difference between the two wall electrodes. Here, for simplicity it was assumed that the electric permitivity coefficient, ε, is constant.

Our objective is to use a single system of governing equations in the entire domain which could locally contain the liquid alone, mixture of the liquid and the solid (mushy region where $T_{liquidus} > T > T_{solidus}$), or the solid alone. Physical properties of the liquid and the solid phases are quite different. The mass fraction of liquid at any point in the domain determines locally to what extent should physical properties of the liquid or the solid phase be taken into account. For example, latent heat released or absorbed per unit mass of the mushy region is proportional to the local volumetric ratio of liquid phase to the entire local volume. This ratio is often modeled (Voller and Swaminathan, 1991) as

$$f = \frac{V_l}{V_l + V_s} = \left(\frac{\theta - \theta_{solidus}}{\theta_{liquidus} - \theta_{solidus}}\right)^n \tag{12}$$

where the exponent n is typically $0.2 < n < 5$. We will assume separate linear variations of density as a function of non-dimensional temperature in the liquid and in the solid. Thus, in the liquid we have

$$\rho_l' = 1 + \left.\frac{\partial(\rho_l/\rho_{ol})}{\partial\theta}\right|_o (\theta - \theta_o) = 1 - \alpha^*_{ol}(\theta - \theta_o) \tag{13}$$

with a similar expression for the liquid simulating the solid phase. For certain materials their physical properties can be significantly different in the liquid as compared to its solid phase. Density, viscosity, heat conductivity, electric charge mobility, electric charge diffusion, and heat capacity in the liquid can be expressed as arbitrary functions of non-dimensional temperature

$$\rho^*_l = \frac{\rho_{ol}}{\rho_o}\rho_l' \quad \mu^*_l = \frac{\mu_{ol}}{\mu_o}\mu_l' \quad k^*_l = \frac{k_{ol}}{k_o}k_l' \quad b^*_l = \frac{b_{ol}}{b_o}b_l' \tag{14}$$

$$D^*_l = \frac{D_{ol}}{D_o}D_l' \quad c^*_l = \frac{c_{ol}}{c_o}c_l' \quad \alpha^*_l = \frac{\alpha_{ol}}{\alpha_o} \quad \varepsilon^*_l = \frac{\varepsilon_{ol}}{\varepsilon_o} \tag{15}$$

with similar expressions for the liquid simulating the solid phase. Here, we assumed thermal expansion coefficients and electric permitivity coefficients to be temperature non-dependent in both liquid and the solid phase. We can now introduce non-dimensional numbers defined as:

Reynolds number

$$Re = \frac{\rho_o\, |\mathbf{v}_o|\, l_o}{\mu_o} \tag{16}$$

Prandtl number

$$Pr = \frac{c_o\, \mu_o}{k_o} \tag{16}$$

Grashof number

$$Gr = \frac{\rho_o^2 |g_o| \alpha_o \Delta T_o l_o^3}{\mu_o^2}$$

Eckert number

$$Ec = \frac{|v_o|^2}{c_o \Delta T_o} \qquad (17)$$

Froude number

$$Fr^2 = \frac{|v_o|^2}{|g_o| l_o}$$

Stefan number

$$S_{te} = \frac{c_o \Delta T_o}{L_o} \qquad (18)$$

Charge diffusivity number

$$D_E = \frac{\mu_o}{\rho_o D_o}$$

Coulomb force number

$$S_E = \frac{q_o \Delta\varphi_o}{\rho_o |v_o|^2} \qquad (19)$$

Electric Prandtl number

$$Pr_E = \frac{\mu_o}{\rho_o b_o \Delta\varphi_o}$$

Electric field number

$$N_E = \frac{q_o l_o^2}{\varepsilon_o \Delta\varphi_o} \qquad (20)$$

Consequently, the non-dimensional system of equations that is valid throughout the computational domain comprising of the liquid, the mushy region and the solid with separate temperature-dependent physical properties in each phase and containing electrically charged particles while under the influence of electrostatic and gravitational arbitrarily oriented external fields can be expressed in a conservative form as:

Mass conservation equation

$$\nabla^* \cdot \mathbf{v}^* = 0 \qquad (21)$$

Linear momentum conservation equation

$$\bar{\bar{\rho}}^* \frac{\partial \mathbf{v}^*}{\partial t^*} + f\,\rho_l^* \nabla^* \cdot (\mathbf{v}^*\mathbf{v}^* + \bar{\bar{p}}_l^* \mathbf{I}) + (1-f)\rho_s^* \nabla^* \cdot (\mathbf{v}^*\mathbf{v}^* + \bar{\bar{p}}_s^* \mathbf{I})$$

$$= f\,\nabla^* \cdot \left(\frac{\mu_l^*}{Re} (\nabla^*\mathbf{v}^* + (\nabla^*\mathbf{v}^*)^T)\right) + \bar{\bar{\alpha}}^* \frac{Gr\ \theta}{Re^2} \mathbf{g}^*$$

$$+ (1-f)\,\nabla^* \cdot \left(\frac{\mu_s^*}{Re} (\nabla^*\mathbf{v}^* + (\nabla^*\mathbf{v}^*)^T)\right) + S_E\, q^* \boldsymbol{E}^* \qquad (22)$$

Energy conservation equation

$$\bar{\bar{c}}^* \frac{\partial \theta}{\partial t^*} + f\,\rho_l^* \nabla^* \cdot (c_{el}^* \theta\, \mathbf{v}^*) + (1-f)\rho_s^* \nabla^* \cdot (c_{es}^* \theta\, \mathbf{v}^*)$$

$$= \frac{1}{RePr} \left(f\,\nabla^* \cdot (k_l^* \nabla^* \theta) + (1-f)\,\nabla^* \cdot (k_s^* \nabla^* \theta) \right)$$

$$+ S_E\, Ec (q^* \mathbf{v}^* \cdot \boldsymbol{E}^* + q^* \bar{\bar{b}}^* \frac{\boldsymbol{E}^* \cdot \boldsymbol{E}^*}{Re\ Pr_E} - \bar{\bar{b}}^* \frac{\nabla^* q^* \cdot \boldsymbol{E}^*}{Re\, D_E}) \qquad (23)$$

Charge conservation equation

$$\frac{\partial q^*}{\partial t^*} + \nabla^* \cdot \left(q^* \left(\mathbf{v}^* + \frac{\bar{\bar{b}}^* \boldsymbol{E}^*}{Re\ Pr_E}\right)\right) = \frac{1}{Re\, D_E} \nabla^* \cdot (\bar{\bar{b}}^* \nabla^* q^*) \qquad (24)$$

and electric potential equation

$$\nabla^{*2} \varphi^* = - N_E\, q^* \left(\frac{f}{\varepsilon_l^*} + \frac{(1-f)}{\varepsilon_s^*}\right) \qquad (25)$$

Here, we used the following symbols for the mixture density, mobility, heat capacity, and thermal expansion

$$\bar{\bar{\rho}}^* = f\,\rho_l^* + (1-f)\,\rho_s^* \qquad \bar{\bar{b}}^* = f\,b_l^* + (1-f)\,b_s^* \qquad (26)$$

$$\bar{\bar{c}}^* = f\,\rho_l^* \frac{\partial (c_{el}^* \theta)}{\partial \theta^*} + (1-f)\,\rho_s^* \frac{\partial (c_{es}^* \theta)}{\partial \theta^*} \qquad (27)$$

$$\bar{\bar{\alpha}}^* = f\,\rho_l^* \alpha_l^* + (1-f)\,\rho_s^* \alpha_s^* \qquad (28)$$

Combination of hydrodynamic and hydrostatic pressures

$$\bar{\bar{p}}_l^* = \frac{p^*}{\rho_l^*} + \frac{\phi^*}{Fr^2} \qquad \text{and} \qquad \bar{\bar{p}}_s^* = \frac{p^*}{\rho_s^*} + \frac{\phi^*}{Fr^2} \qquad (29)$$

uses the non-dimensional gravity potential ϕ^* defined as $\mathbf{g}^* = \nabla^* \phi^*$. We used an enthalpy method to formulate the equivalent specific heat coefficients in the liquid and the solid phases as $c_{el}^* = c_l^* - \frac{1}{S_{te}} \frac{\partial f}{\partial \theta}$ and $c_{es}^* = c_s^* - \frac{1}{S_{te}} \frac{\partial f}{\partial \theta}$, respectively. Notice that this expression allows for the latent heat not to be a constant, but to be released in the mushy region according to the empirical law given in equation (12). According to the Boussinesq approximation, viscous dissipation can be neglected (Gray and Giorgini, 1976; Lee, Dulikravich and Kosovic, 1991) since its ratio with respect to the convective term in the energy equation is of the order $\frac{Ec}{Re}$ which is typically a very small number.

EHD SOLIDIFICATION: NUMERICAL MODEL

The non-dimensional system of governing equations (21-24) can be written in a fully conservative vector form in

physical Cartesian x,y coordinates as follows

$$\mathbf{D}^* \frac{\partial \mathbf{Q}^*}{\partial t^*} + f\,\rho_l^* \left(\frac{\partial \mathbf{E}^{*l}}{\partial x^*} + \frac{\partial \mathbf{F}^{*l}}{\partial y^*}\right) + (1-f)\,\rho_s^* \left(\frac{\partial \mathbf{E}^{*s}}{\partial x^*} + \frac{\partial \mathbf{F}^{*s}}{\partial y^*}\right)$$

$$= \mathbf{D}_{NS}^* \Big[f \left(\frac{\partial}{\partial x^*}\left(\mathbf{D}_{NS}^{*l} \frac{\partial \mathbf{Q}^*}{\partial x^*}\right) + \frac{\partial}{\partial y^*}\left(\mathbf{D}_{NS}^{*l} \frac{\partial \mathbf{Q}^*}{\partial y^*}\right)\right)$$

$$+ (1-f) \left(\frac{\partial}{\partial x^*}\left(\mathbf{D}_{NS}^{*s} \frac{\partial \mathbf{Q}^*}{\partial x^*}\right) + \frac{\partial}{\partial y^*}\left(\mathbf{D}_{NS}^{*s} \frac{\partial \mathbf{Q}^*}{\partial y^*}\right)\right)\Big] + \mathbf{S}^* \qquad (30)$$

where the solution vector $\mathbf{Q}^*$ and the vectors $\mathbf{E}^{*l}$, $\mathbf{F}^{*l}$ are

$$\mathbf{Q}^* = \{\, 0 \;\; u^* \;\; v^* \;\; \theta \;\; q^* \,\}^T \qquad (31)$$

$$\mathbf{E}^{*l} = \begin{Bmatrix} u^* \\ u^{*2} + \bar{\bar{p}}_l^* \\ u^* v^* \\ u^* \theta \\ b_l^* E_x^* \\ q^*\left(u^* + \dfrac{}{\mathrm{RePr}_E}\right) \end{Bmatrix} \qquad \mathbf{F}^{*l} = \begin{Bmatrix} v^* \\ v^* u^* \\ v^{*2} + \bar{\bar{p}}_l^* \\ v^* \theta \\ b_l^* E_y^* \\ q^*\left(v^* + \dfrac{}{\mathrm{RePr}_E}\right) \end{Bmatrix} \qquad (32)$$

with similar expressions for $\mathbf{E}^{*s}$ and $\mathbf{F}^{*s}$. The source vector is

$$\mathbf{S}^* = \begin{Bmatrix} 0 \\ \bar{\bar{\alpha}}^* \dfrac{Gr\,\theta}{Re^2} g_x^* + S_E\, q^*\, E_x^* \\ \bar{\bar{\alpha}}^* \dfrac{Gr\,\theta}{Re^2} g_y^* + S_E\, q^*\, E_y \\ S_E\, Ec \left(q^* \mathbf{v}^* \cdot \boldsymbol{E}^* + q^*\, \bar{\bar{b}}^* \dfrac{\boldsymbol{E}^* \cdot \boldsymbol{E}^*}{Re\, Pr_E} - \bar{\bar{b}}^* \dfrac{\nabla^* q^* \cdot \boldsymbol{E}^*}{Re\, D_E}\right) \\ 0 \end{Bmatrix} \qquad (33)$$

Here, diagonal coefficient matrices are

$$\mathbf{D}^* = \mathrm{diag}\left[1 \;\; \bar{\bar{\rho}} \;\; \bar{\bar{\rho}} \;\; \bar{\bar{c}} \;\; 1\right] \qquad \mathbf{D}_{NS}^* = \mathrm{diag}\left[0 \;\; \frac{1}{Re} \;\; \frac{1}{Re} \;\; \frac{1}{RePr} \;\; \frac{1}{ReD_E}\right] \qquad (34)$$

$$\mathbf{D}_{NS}^{*l} = \mathrm{diag}\left[0 \;\; \mu_l^* \;\; \mu_l^* \;\; k_l^* \;\; b_l^*\right] \qquad \mathbf{D}_{NS}^{*s} = \mathrm{diag}\left[0 \;\; \mu_s^* \;\; \mu_s^* \;\; k_s^* \;\; b_s^*\right] \qquad (35)$$

For the purpose of developing a versatile EHD solidification/melting analysis code applicable to arbitrary configurations where correct boundary conditions could be easily enforced precisely at the boundaries, the system of equations (30) was transformed in a fully conservative vector form expressed in general curvilinear boundary-conforming non-orthogonal coordinates (ξ,η) (Lee, Dulikravich and Kosovic, 1991; Dulikravich, Ahuja and Lee, 1993a; 1993b) as

$$\mathbf{D}^* \frac{\partial \tilde{\mathbf{Q}}^*}{\partial t^*} + f \left(\frac{\partial \tilde{\mathbf{E}}^{*l}}{\partial \xi^*} + \frac{\partial \tilde{\mathbf{F}}^{*l}}{\partial \eta^*}\right) + (1-f) \left(\frac{\partial \tilde{\mathbf{E}}^{*s}}{\partial \xi^*} + \frac{\partial \tilde{\mathbf{F}}^{s}}{\partial \eta^*}\right)$$

$$= \mathbf{D}_{NS}^* \Big[f \left(\frac{\partial}{\partial \xi^*}\left(\frac{\mathbf{D}_{NS}^{*l}}{J} g_{ij} \frac{\partial J \tilde{\mathbf{Q}}^*}{\partial \xi^*}\right) + \frac{\partial}{\partial \eta^*}\left(\frac{\mathbf{D}_{NS}^{*l}}{J} g_{ij} \frac{\partial J \tilde{\mathbf{Q}}^*}{\partial \eta^*}\right)\right) + \mathbf{S}^*$$

$$+ (1-f) \left(\frac{\partial}{\partial \xi^*}\left(\frac{\mathbf{D}_{NS}^{*s}}{J} g_{ij} \frac{\partial J \tilde{\mathbf{Q}}^*}{\partial \xi^*}\right) + \frac{\partial}{\partial \eta^*}\left(\frac{\mathbf{D}_{NS}^{*s}}{J} g_{ij} \frac{\partial J \tilde{\mathbf{Q}}^*}{\partial \eta^*}\right)\right)\Big] \qquad (36)$$

where

$$\tilde{\mathbf{Q}}^* = \frac{1}{J} \left\{ \frac{p^*}{\beta} \;\; u^* \;\; v^* \;\; \theta \;\; q^* \right\}^T \qquad (37)$$

$$\tilde{\mathbf{E}}^{*l} = \frac{1}{J} \begin{Bmatrix} U^* \\ U^* u^* + \xi_{,x}\, \bar{\bar{p}}_l^* \\ U^* v^* + \xi_{,y}\, \bar{\bar{p}}_l^* \\ U^* \theta \\ b_l^* E_\xi^* \\ \theta\left(U^* + \dfrac{}{\mathrm{RePr}_E}\right) \end{Bmatrix} \qquad \tilde{\mathbf{F}}^{*l} = \frac{1}{J} \begin{Bmatrix} V^* \\ V^* u^* + \eta_{,x}\, \bar{\bar{p}}_l^* \\ V^* v^* + \eta_{,y}\, \bar{\bar{p}}_l^* \\ V^* \theta \\ b_l^* E_\eta^* \\ \theta\left(V^* + \dfrac{}{\mathrm{RePr}_E}\right) \end{Bmatrix} \qquad (38)$$

Here, $J = \det[\partial(\xi,\eta)/\partial(x,y)]$ and g_{ij} is the metric tensor given by $g_{ij} = \nabla x_i' \cdot \nabla x_j'$, while U^* and V^* are the non-dimensionalized contravariant velocity vector components. A non-physical term, $\dfrac{\partial (p^*/\beta)}{\partial t^*}$, representing an artificial compressibility (Chorin, 1967) was added so that the system (30) can be made non-singular and consequently integrated in time simultaneously. The parameter β is a constant

specified by the user. It depends on the Reynolds number and computational grid clustering, orthogonality and smoothness (Lee and Dulikravich, 1991). The artificial compressibility concept is more consistent and easier to code than an equally common pressure-based algorithm for incompressible Navier-Stokes equations. The system of coupled nonlinear partial differential equations (36) was discretized using central differencing and integrated iteratively using a four-stage explicit Runge-Kutta time stepping (Jameson et al., 1981) given as

$$\begin{aligned} \tilde{Q}^{o} &= \tilde{Q}^{n} \\ \Delta \tilde{Q}^{m} &= -\gamma_m \Delta t \; \tilde{R}^{m-1} \qquad m = 1,2,3,4 \\ \tilde{Q}^{n+1} &= \tilde{Q}^{n} + \Delta \tilde{Q}^{4} \end{aligned} \tag{39}$$

where the iteration level is denoted by n, and each stage of the Runge-Kutta algorithm by m. Here the coefficients are γ_m = 1/4, 1/3, 1/2 and 1, respectively. The residual vector $\tilde{R}$ is computed by moving all terms from the right side of the system (36) to its left side and explicitly adding a fourth order artificial dissipation defined as (Steger and Kutler, 1977)

$$-\frac{\varepsilon_4 \psi}{4 J \Delta t}\left(\frac{\partial^4}{\partial \xi^{*4}} + \frac{\partial^4}{\partial \eta^{*4}}\right)(J\tilde{Q}^{*}) \tag{40}$$

to stabilize the algorithm which is otherwise prone to oscillations due to even-odd decoupling because it uses central differencing in space. The sensor function ψ was based on normalized second derivative of electric charge distribution. Poisson's equation (25) for electric potential was solved separately during each global iteration using a fast alternating-direction implicit algorithm. Wall boundary conditions for the pressure were computed from the normal momentum equation. Boundary conditions for electric charges on the electrically isolated boundaries were of the Neumann type. Otherwise, electric charges were injected uniformly at one boundary and their pattern was computed at the opposite boundary.

NUMERICAL RESULTS

Based on our theoretical model and the numerical algorithm, a FORTRAN code was developed capable of predicting details of the convection and conduction heat transfer in EHD flows involving solidification/melting. Although the code is applicable to arbitrary two-dimensional configurations, for the purpose of analyzing the fundamental phenomenas we chose to numerically test solidification processes in a simple configuration consisting of a closed horizontal two-dimensional rectangular container of aspect ratio 2:1 (l_o = 0.033333 [m] in height) fully filled with the molten gallium arsenide (Brodsky, 1990; Sabhapathy and Salcudean, 1990). The container area was discretized with a symmetrically clustered orthogonal computational grid of 60 × 60 rectangular grid cells. Physical properties used in this work are summarized in Table 1 and the corresponding non-dimensional numbers are given in Table 2. Certain properties were estimated based on the analytical relations given by Eringen and Maugin (1990) and by Kuffel and Zaengl (1984). For example, since we did not have reliable information as to the typical level of the electric charges and mobilities, we used $q_o = 1 \times 10^{-4}$ [C m^{-3}] and $b_o = 1 \times 10^{-8}$ [m^2 V^{-1} s^{-1}] as the reference values which correspond to an aqueous biological solution (Saville and Palusinski, 1986). Since there is no mean velocity in this type of flows, we defined Reynolds number as $Re = (Gr)^{0.5}$ which determines the reference velocity in full gravity as v_o = 0.02473 [m s^{-1}] and in reduced gravity test cases as v_o = 0.002473 [m s^{-1}]. All other reference values used in the non-dimensionalization corresponded to the liquidus temperature (Table 1). The following non-dimensional numbers were used in all the test cases: Pr = 0.068, Ste = 5.98 x10^{-3}, DE = 1.95 x10^{-4}. Top wall was specified as uniformly cold at θ = - 0.5 (T_{cold} = 1505.995 [K]), bottom wall was uniformly hot at θ = 0.5 (T_{hot} = 1515.995 K), while vertical walls were adiabatic. Gravity vector was applied vertically downward. The user-specified parameter ε_4 in the fourth order artificial dissipation was ε_4 = 0.0005. Initial guesses were $\mathbf{v}$ = 0, p = 0, θ = 0.5, q = q_o (or q = 0), and $\boldsymbol{E}$ = constant (or $\boldsymbol{E}$ = 0). Several distinct test cases were numerically analyzed.

Case 1: There was no electric field applied in this case and no charged particles were introduced while full gravity force was applied. This is the typical case of solidification from above where two strong thermo-convective counter rotating vortices (Fig. 1a) exist in the steady state situation below the solid that accrued on the top wall. Strong temperature gradients exist inside the solid and the solid/liquid interface is highly curved (Fig. 1b). Due to the strong convection in this test case the computed normal temperature gradients (negative) at the bottom wall and at the top wall are highly nonuniform (Fig. 1c). Notice that differences in the magnitudes of the arrows in Figure 1c at the top and bottom walls are due to the fact that thermal conductivities of liquid and solid GaAs are quite different (Table 1). This case resulted in 579 solid cells. When running this same test case with 1% of terrestrial gravity ($\mathbf{g}^*$ = 0.01), only mild convection started initially. Nevertheless, as the solidification front advanced downwards from the top wall the effective melt height reduced thus strongly reducing Gr and the effective Rayleigh number (Ra = Gr Pr). Consequently, the effective Ra number became subcritical and thermal covection ceased altogether. As a result, this test case produced a steady state with pure conduction in the accrued solid and in the melt below. The predicted isotherms were practically horizontal and the number of predicted solidified computational cells was 1217.

Case 2: A uniform external electrostatic field of 5000 V was applied in this case acting downwards as was the full gravity

force. We assumed that the charged particle concentration was uniform at the lower wall while treating the top wall as an exit boundary for the charged particles since the side walls had a Neumann condition imposed on electric charges. Negligible differences between the results in this case and in the previous case have been observed. Specifically, the computed velocity field (Fig. 2a), temperature field (Fig. 2b) and the normal derivatives (negative) of temperature at the top and the bottom walls (Fig. 2c) are practically the same as in Figures 1a, 1b and 1c. Consequently, an almost identical number of 566 solidified computational cells was predicted. This is due to the strong thermal convection that exists in the full gravity suggesting that a stronger electric field is needed for its control.

Case 3: A uniform external electrostatic field of 5000 V was applied in this case acting downwards as was a low normalized gravity force of $g^* = 0.01$. We enforced a uniform distribution of the charged particles at the lower wall while treating the top wall as an exit boundary for the charged particles since the side walls had a Neumann condition imposed on electric charges. The resulting Coulomb force in this case was strong enough to overcome the viscous force and cause a pure electro-convection (Fig. 5a) consisting of two weak counter-rotating vortices. The predicted isotherms (Fig. 5b) are mildly curved, while the predicted normal temperature derivatives at the top and the bottom walls (Fig. 5c) are only mildly non-uniform. There were 1206 solidified computational cells predicted in this test case.

Case 4: In this case an external electrostatic field of 15000 V was applied horizontally while full gravity acted vertically downwards. A uniform electric charge density was specified at the left vertical wall, normal derivatives of charges were zero at the top and the bottom walls, and charges were computed at the right vertical wall. Because of the strong interaction of thermal buoyancy and the electro-convection, this case resulted in a highly asymmetric solution containing a complex pattern of counter-rotating vortices (Fig. 3a). The asymmetry is obvious in the predicted thermal field (Fig. 3b) and the corresponding normal temperature derivatives at the top and the bottom walls (Fig. 3c). This test case resulted in 609 solidified computational cells.

Case 5: In this case an external electrostatic field of 10000 V was applied horizontally while reduced gravity ($g^* = 0.01$) acted vertically downwards. The electric charges were specified as uniform at the left vertical wall. A dramatic change of pattern of the resulting electro-convection consisted of a single asymmetric vortex (Fig. 6a) causing also a slight asymmetry in the predicted isotherm pattern (Fig. 6b) and the normal temperature derivatives at the top and the bottom walls (Fig. 6c). In this case there were 1195 solidified computational cells predicted.

CONCLUSIONS

A complex analytical model capable of simultaneously capturing thermo-convective and electro-convective motion inside a liquid, details of the mushy region, and the accrued solid phase has been successfully numerically implemented for the cases with electrically charged particles and arbitrary externally applied electrostatic and gravitational fields. Numerical simulation of two-dimensional solidification from above of a GaAs melt reveals that the electrostatic field has definite consequences on the thermal field inside the melt and the solid accrued because of the creation of electro-convection. Consequently, predicted wall heat fluxes with the applied electrostatic field differ significantly from those without the electric field. These effects are more pronounced in the reduced gravity than in the full gravity environment for low Rayleigh numbers. Computational results indicate extreme importance of understanding the interplay between the externally imposed electric and gravitational field strengths and orientations. If the solidification process had been simulated with a time-accurate code, precise impurities deposition pattern inside the solid could be predicted. This suggests possibilities to develop an algorithm for a judicious application of the external electric field to actively control impurities or dopant deposition pattern in the crystal, heat transfer, the amount of solid accrued and the solid/liquid interface shape.

ACKNOWLEDGMENTS

Computing time was provided by NASA Lewis Research Center for remotely accessing Cray C-90 computer at NAS facility of NASA Ames Research Center. Post processing was performed on equipment donated by the Apple Computer, Inc.

REFERENCES

Babskii, V. G., Zhukov, M. Y. and Yudovich, V. I., 1989, "Mathematical Theory of Electrophoresis", (translated by C. Flick), Consultants Bureau, New York, N.Y.

Bello, M. S. and Polezhaev, V. I., 1991, "Hydrodynamics, Gravitational Sensitivity and Transport Phenomena in Continuous Flow Electrophoresis", AIAA paper 91-0112, Aerospace Sciences Meeting, Reno, Nevada, January 7-10, 1991.

Brodsky, M. H., 1990. "Properties of Gallium Arsenide", 2nd edition, INSPEC, EMIS Datareview Series No. 2.

Chorin, A. J., 1967, "A Numerical Method for Solving Incompressible Viscous Flow Problems", *Journal of Computational Physics*, Vol. 2, pp. 12-26.

Dulikravich, G. S., Ahuja, V. and Lee, S., 1993a, "Computation of Electro-Thermo-Convective Phenomena in Electro-Rheological Fluids", ASME Fluids Engineering Summer Meeting, Proceedings of Symposium on Electro-Rheological Flows, Editors: D. A. Siginer, J. H. Kim and R. A. Bajura, Washington, D. C., June 21-24, 1993, ASME FED-Vol. 164, pp. 29-42.

Dulikravich, G. S., Ahuja, V. and Lee, S., 1993b, "Simulation of Electrohydrodynamic Enhancement of Laminar Flow Heat Transfer", ASME National Heat Transfer Conference, Atlanta, Georgia, August 8-11, 1993; also in *Journal of Enhanced Heat Transfer*, Vol. 1, No. 1, August 1993.

Dulikravich, G. S., Ahuja, V. and Lee, S., 1993c. "Three-Dimensional Solidification With Magnetic Fields and Reduced Gravity", AIAA paper 93-0912, Reno, Nevada, January 11-14, 1993; also to appear in *International Journal of Heat and Mass Transfer*.

Dulikravich, G. S. and Kosovic, B., 1992, "Solidification of Variable Property Melts Under the Influence of Low Gravity, Magnetic Fields and Electric Fields," AIAA paper 92-0694, AIAA Aerospace Sciences Meeting, Reno, Nevada, January 6-9, 1992.

Eringen, A. C., and Maugin, G. A., 1990, *Electrodynamics of Continua II; Fluids and Complex Media*, Springer-Verlag, New York, N.Y., pp. 562-563.

Fernandez, J. L., and Poulter, R., 1987, "Radial Mass Flow in Electrohyhrodynamically-Enhanced Forced Heat Transfer in Tubes", *International Journal of Heat and Mass Transfer*, Vol. 30, No. 10, pp. 2125-2136.

Fujino, T., Yokoyama, Y., and Mori, Y. H., 1989, "Augmentation of Laminar Forced Convection Heat Transfer by Application of a Transverse Electric Field", *Journal of Heat Transfer*, Vol. 111, pp. 345-351.

Gray, D. D., and Giorgini, A., 1976, "The Validity of the Bousinessq Approximation for Liquids and Gases", *International Journal of Heat and Mass Transfer*, Vol. 19, pp. 545-551.

Hosseini-Sianaki, A., Firoozian, R., Peel, D. J. and Bullough, W.A., 1992, "Comparative Methods for the Derivation of In Flow Electrical Characteristics of Electro-Rheological Fluids", *Journal of Intelligent Material Systems and Structures*, Vol. 3, pp. 96-111.

Jameson, A., Schmidt, W., and Turkel, E., 1981, "Numerical Solutions of the Euler Equations by Finite Volume Methods Using Runge-Kutta Time-Stepping Scheme", AIAA paper 81-1259, Palo Alto, CA, June 1991.

Kuffel, E. and Zaengl, W. S., 1984, *High Voltage Engineering Fundamentals*, Pergamon Press, Oxford.

Landau, L. D. and Lifshitz, E. M., 1960, "Electrodynamics of Continuous Media", Pergamon Press, New York.

Lee, S. and Dulikravich, G. S., 1991, "Performance Analysis of DMR Method for Acceleration of Iterative Algorithms," AIAA paper 91-0241, AIAA Aerospace Sciences Meeting, Reno, Nevada, January 7-10, 1991.

Lee, S., Dulikravich, G. S. and Kosovic, B., 1991, "Electrohydrodynamic (EHD) Flow Modeling and Computations", AIAA Paper 91-1469, AIAA Fluid, Plasma Dynamics and Lasers Conference, Honolulu, Hawaii, June 24-26, 1991.

Melcher, J. R., 1981, "Continuum Electromechanics", The MIT Press, Cambridge, Massachussetts.

Ohadi, M. M., 1991, "Heat Transfer Enhancement in Heat Exchangers", *ASHRAE Journal*, Vol. 33, No. 12, pp. 42-50.

Sabhapathy, P. and Salcudean, M. E., 1990, "Numerical Study of Flow and Heat Transfer in LEC Growth of GaAs With an Axial Magnetic Field", *Journal of Crystal Growth*, Vol. 104, pp. 371-388.

Steger, J. L. and Kutler, P., 1977, "Implicit Finite-Difference Procedure for the Computation of Vortex Wakes", *AIAA Journal*, Vol. 15, No. 7, pp. 581-590.

Stuetzer, O. M., 1962, "Magnetohydrodynamics and Electrohydrodynamics", *The Physics of Fluids*, Vol. 5, No. 5, pp. 534-544.

Voller V. R. and Swaminathan, C. R., 1991, "General Source-Based Method for Solidification Phase Change", *Numerical Heat Transfer, Part B*, Vol. 19, pp. 175-189 .

Zahn, M. and Chatelon, H., 1977, "Charge Injection Between Concentric Cylindrical Electrodes", *Journal of Applied Physics*, Vol. 48, No. 5, pp. 1797-1805.

Physical property	Numerical value	Source
ρ_{ol} [kg m^{-3}]	5710	c
ρ_{os} [kg m^{-3}]	5196	a (page 1.1)
c_{ol} [J kg^{-1} K^{-1}]	434	c
c_{os} [J kg^{-1} K^{-1}]	416	a (page 1.8)
k_{ol} [W m^{-1} K^{-1}]	17.8	c
k_{os} [W m^{-1} K^{-1}]	7.0	c
T_{ol} [K]	1511	c
T_{os} [K]	1510.995	c
b_{ol} [m^2 V^{-1} s^{-1}]	1×10^{-8}	e
b_{os} [m^2 V^{-1} s^{-1}]	1×10^{-10}	assumed
D_{ol} [m^2 s^{-1}]	2.5×10^{-1}	b (page562)
D_{os} [m^2 s^{-1}]	2.5×10^{-14}	assumed
α_{ol} [K^{-1}]	1.87×10^{-4}	c
α_{os} [K^{-1}]	7.95×10^{-6}	a (page 1.7)
μ_{ol} [kg m^{-1} s^{-1}]	2.79×10^{-3}	c
μ_{os} [kg m^{-1} s^{-1}]	2.79×10^{2}	specified
ε_{ol} [kg m $s^{-2}V^{-2}$]	1×10^{-10}	e
ε_{os} [kg m $s^{-2}V^{-2}$]	1×10^{-10}	assumed
L_o [J kg^{-1}]	726 000	c

Table 1. Physical properties for GaAs: a) Brodsky, b) Eringen and Maugin, c) Sabhapathy and Salcudean, d) Kuffel and Zaengl, e) Saville and Palusinski.

	Case no.1	Case no.2	Case no.3	Case no.4	Case no.5
g	1	1	0.01	1	0.01
$\Delta\varphi$(V)	0	5000 ↑	5000 ↑	15000 →	10000 →
Re	1687	1687	168.7	1687	168.7
Gr	2.85×10^6	2.85×10^6	2.85×10^4	2.85×10^6	2.85×10^4
Ec	1.41×10^{-7}	1.41×10^{-7}	1.41×10^{-9}	1.41×10^{-7}	1.41×10^{-9}
N_E	-NA-	0.222	0.222	0.07407	0.111
S_E	-NA-	0.143	14.3	0.429	28.6
Pr_E	-NA-	9.77×10^{-3}	9.77×10^{-3}	3.26×10^{-3}	4.88×10^{-3}

Table 2. Input parameters for EHD solidification of GaAs melt in a 2:1 aspect ratio closed container. Arrows designate orientation of the uniform electrostatic field vector E.

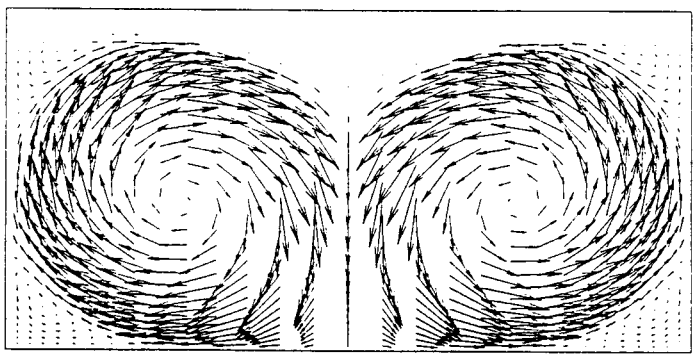

Figure 1a. Case 1: Velocity vector field due to thermo-convection in full gravity without electric field and charged particles. Solid accrues from top wall.

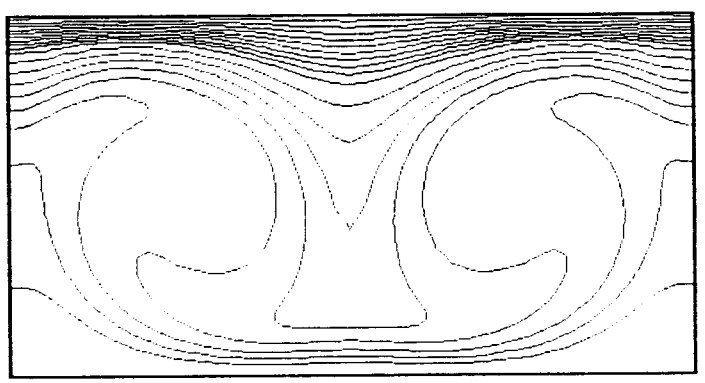

Figure 1b. Case 1: Isotherms in the accrued solid and in the melt due to thermo-convection in full gravity without electric field and charged particles.

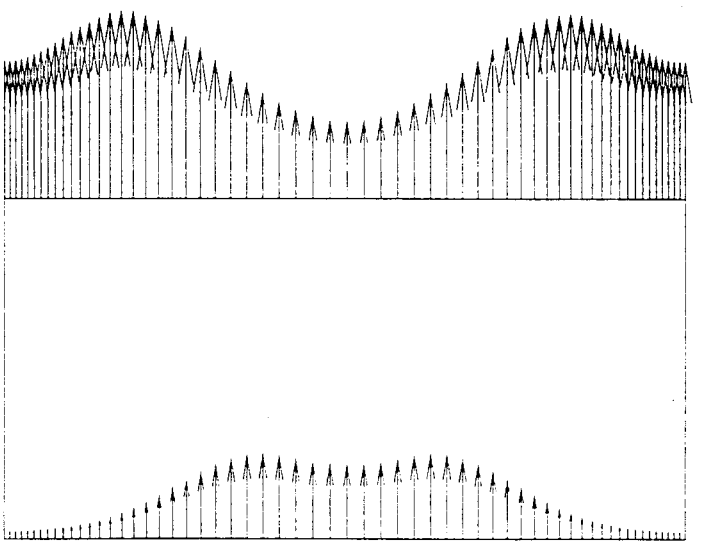

Figure 1c. Case 1: Normal temperature derivatives (negative) on the top and the bottom walls due to thermo-convection in full gravity without an electric field and charged particles.

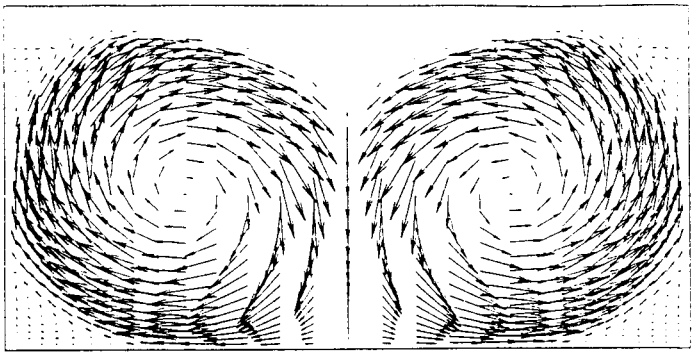

Figure 2a. Case 2: Velocity vector field due to combined thermo-convection and electro-convection in full gravity. Electric field ($\Delta\varphi$ = 5000 V) acts vertically upwards. Solid accrues from top wall.

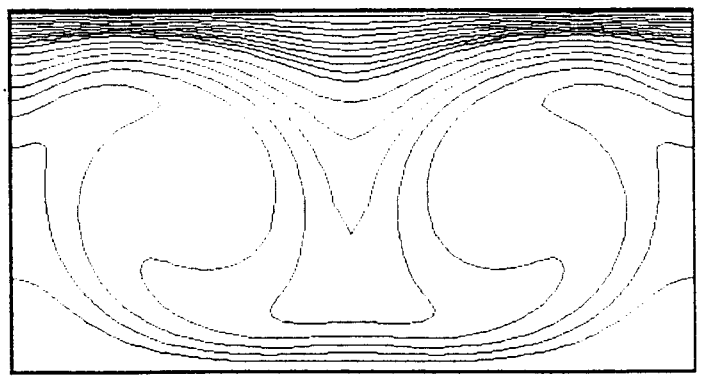

Figure 2b. Case 2: Isotherms in the accrued solid and in the melt due to thermo-convection and electro-convection in full gravity. Electric field ($\Delta\varphi$ = 5000 V) acts vertically upwards. Solid accrues from top wall.

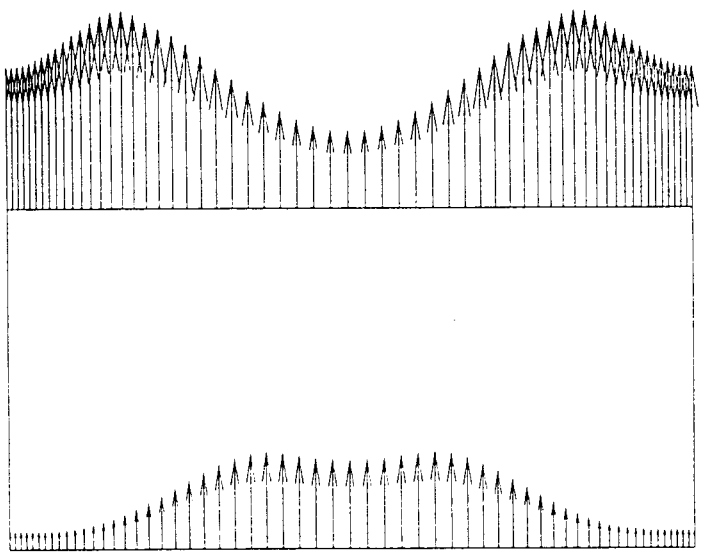

Figure 2c. Case 2: Normal temperature derivatives (negative) on the top and the bottom walls due to thermo-convection and electro-convection in full gravity. Electric field ($\Delta\varphi$ = 5000 V) acts vertically upwards. Solid accrues from top wall.

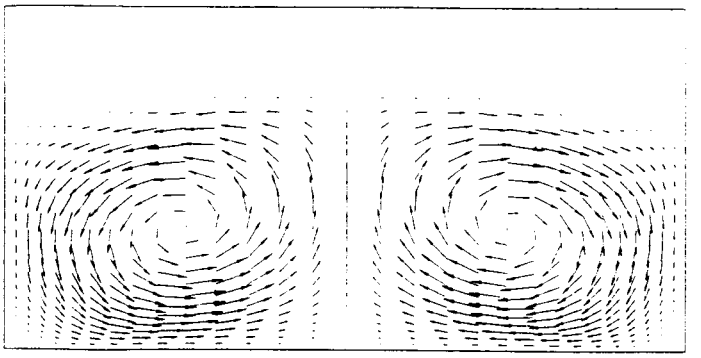

Figure 3a. Case 3: Velocity vector field due to electro-convection in reduced gravity. Electric field ($\Delta\varphi$ = 5000 V) acts vertically upwards. Solid accrues from top wall.

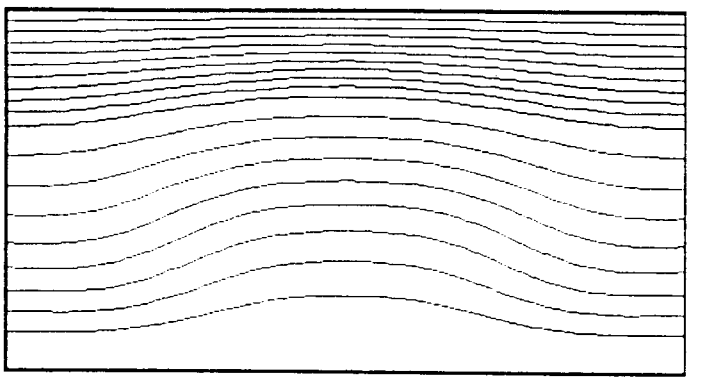

Figure 3b. Case 3: Isotherms in the accrued solid and in the melt due to electro-convection in reduced gravity. Electric field ($\Delta\varphi$ = 5000 V) acts vertically upwards. Solid accrues from top wall.

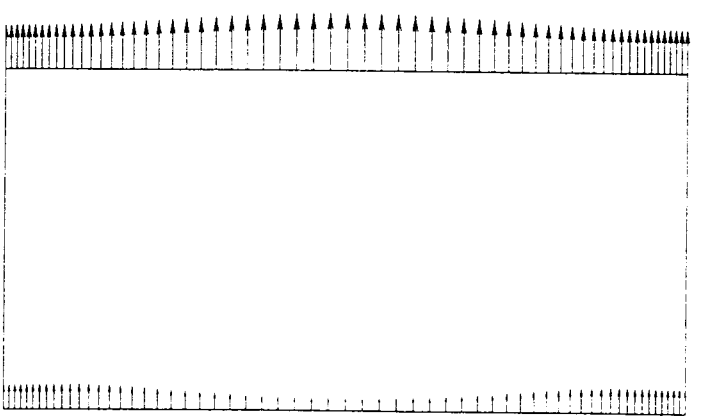

Figure 3c. Case 3: Normal temperature derivatives (negative) on the top and the bottom walls due to electro-convection in reduced gravity. Electric field ($\Delta\varphi$ = 5000 V) acts vertically upwards. Solid accrues from top wall.

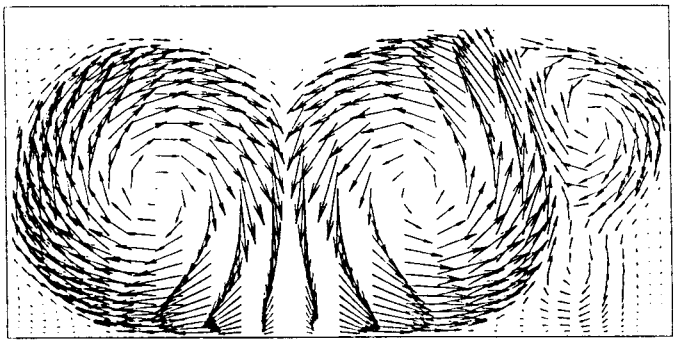

Figure 4a. Case 4: Velocity vector field due to combined thermo-convection and strong electro-convection in full gravity. Electric field ($\Delta\varphi$ = 15000 V) acts horizontally from left to right. Solid accrues from top wall.

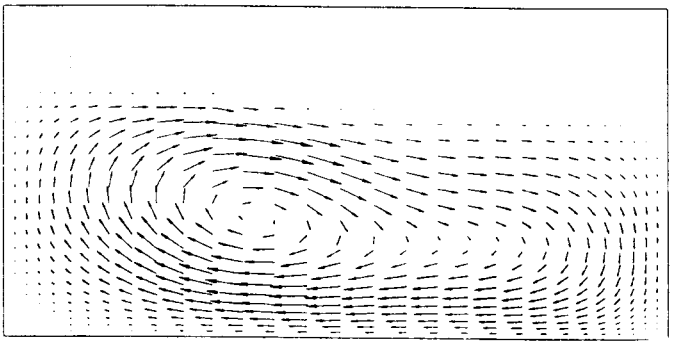

Figure 5a. Case 5: Velocity vector field due to electro-convection in reduced gravity. Electric field ($\Delta\varphi$ = 10000 V) acts horizontally from left to right. Solid accrues from top wall.

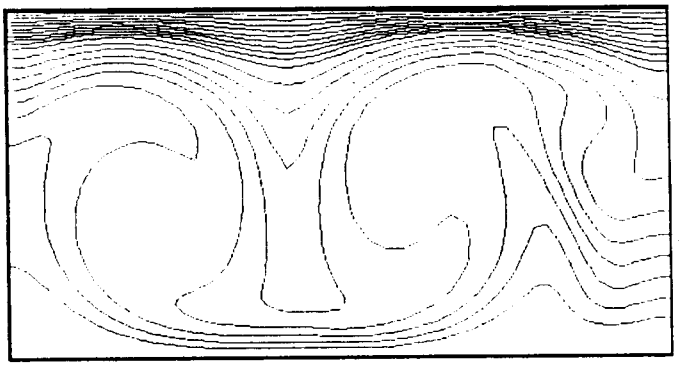

Figure 4b. Case 4: Isotherms in the accrued solid and in the melt due to thermo-convection and strong electro-convection in full gravity. Electric field ($\Delta\varphi$ = 15000 V) acts horizontally from left to right. Solid accrues from top wall.

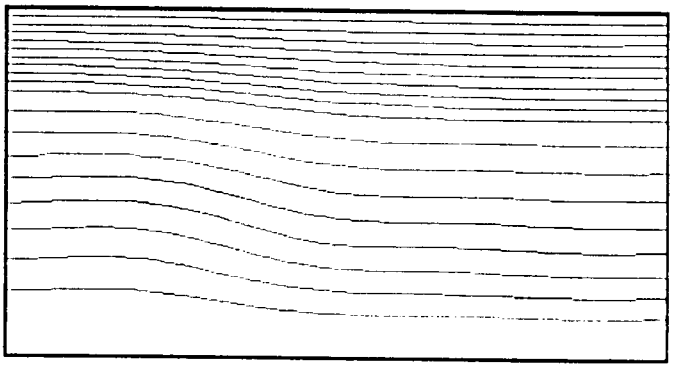

Figure 5b. Case 5: Isotherms in the accrued solid and in the melt due to electro-convection in reduced gravity. Electric field ($\Delta\varphi$ = 10000 V) acts horizontally from left to right. Solid accrues from top wall.

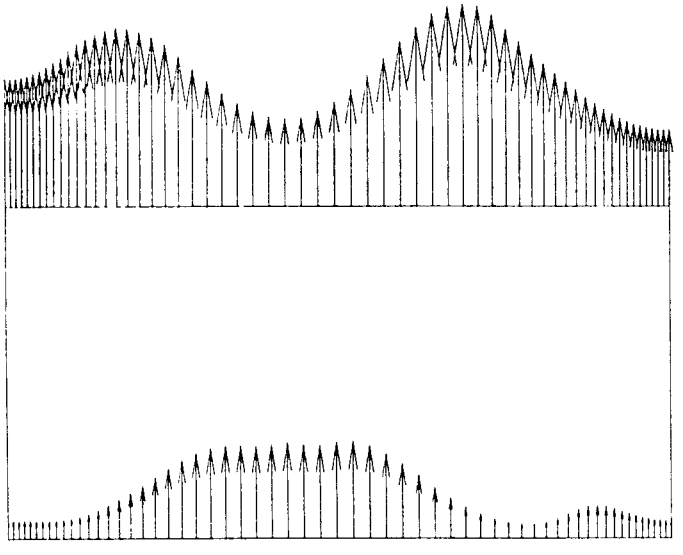

Figure 4c. Case 4: Normal temperature derivatives (negative) on the top and the bottom walls due to thermo-convection and strong electro-convection in full gravity. Electric field ($\Delta\varphi$ = 15000 V) acts horizontally from left to right. Solid accrues from top wall.

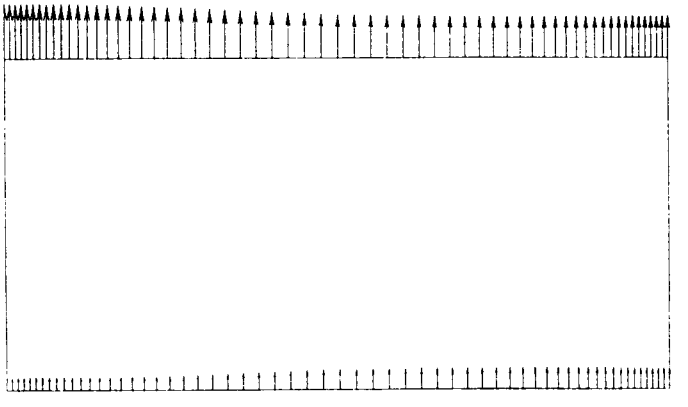

Figure 5c. Case 5: Normal temperature derivatives (negative) on the top and the bottom walls due to electro-convection in reduced gravity. Electric field ($\Delta\varphi$ = 10000 V) acts horizontally from left to right. Solid accrues from top wall.